Post-print of: Głowienka D., Miruszewski T., Szmytkowski J.: The domination of ionic conductivity in tetragonal phase of the organometal halide perovskite CH3NH3PbI3-xClx. SOLID STATE SCIENCES. Vol. 82, (2018), p. 19-23. DOI: 10.1016/j.solidstatesciences.2018.05.009

The Domination of Ionic Conductivity in Tetragonal Phase of the Organometal Halide Perovskite $CH_3NH_3PbI_{3-x}Cl_x$

Damian Głowienka, Tadeusz Miruszewski, Jędrzej Szmytkowski

Faculty of Applied Physics and Mathematics, Gdańsk University of Technology Narutowicza 11/12, 80-233 Gdańsk, Poland

Abstract

Organometal trihalide perovskites have recently gained extreme attention due to their high solar energy conversion in photovoltaic cells. Here, we investigate the contribution of iodide ions to a total conductivity of the mixed lead halide perovskite $CH_3NH_3PbI_{3-x}Cl_x$ with a use of the modified DC Hebb–Wagner polarization method. It has been identified that an ionic conductivity dominates in tetragonal phase which is associated with room temperature. The obtained activation energy for this type of hopping mechanism is equal to (0.87 ± 0.02) eV, which is in a good agreement with previous literature reports. The high contribution of ionic conductivity at room temperature might be a reason of the observed hysteresis in halide perovskite solar cells.

Keywords: $CH_3NH_3PbI_{3-x}Cl_x$, perovskites, hybrid solar cells, ionic conductivity, electronic conductivity

1. INTRODUCTION

Organometal trihalide perovskites are relatively new photovoltaic materials. However, in a short period of intensive progress, an efficiency of solar cells based on these perovskites has already increased to over 20 % [1, 2]. Extraordinary properties leading to such a high efficiency have been connected mainly with a high absorption coefficient in a wide spectrum of light [3], a high mobility of charge carriers [4], a low exciton binding energy at room temperature [5, 6] and a long electron–hole diffusion length [7]. The theoretical maximum efficiency of the perovskite solar cells is estimated to be over 30 % [8, 9]. In order to improve the performance, all physical phenomena which take place in these systems must be well understood. The analysis of current–voltage characteristics demonstrates the effect of rate–dependent hysteresis in numbers of such

Email addresses: dglowienka@mif.pg.gda.pl (Damian Głowienka), tmiruszewski@mif.pg.gda.pl (Tadeusz Miruszewski), jedrek@mif.pg.gda.pl (Jędrzej Szmytkowski)

structures [10, 11, 12]. Therefore, the understanding of the major mechanism influencing the hysteresis effect is crucial for future development of the perovskite solar cells. According to Snaith *et al.* [10] there are three possible explanations of the hysteresis: (1) the large density of defect states at the interface, (2) ferroelectric properties and slow polarization of the material, and (3) the polarization–dependent moveable ions which can screen a space charge buildup that influences the charge collection at the contacts. The fourth possible scenario was suggested by Cojocaru et al. [13] where the electrical capacitance could also explain a hysteresis effect. The previous studies suggest that the interfacial trapping and detrapping processes cannot be the source of hysteresis by themselves as they occur at timescale of miliseconds and that is too fast comparing to I–V hysteresis characterized by seconds to minute timescale [12, 14, 15]. According to authors of the recent papers, the space group of tetragonal phase is polar and therefore the halide perovskites are ferroelectric [16, 17]. However the time which characterizes the rate of ferroelectric domain (0.1–1 ms) estimated by Leguy *et al.* shows that the ferroelectric polarization is not the source of hysteresis solely [18]. Tress *et al.* [15] have reported that ions accumulate at the interface of electrodes and screen the built–in electric field independently of illumination. Their conclusion was that the ionic flow with timescale of seconds to minutes could create the I–V hysteresis dependently of voltage sweep rate. However, besides the influence of ion migration on hysteresis effect, there is also evidence that ionic conductivity of $CH_3NH_3PbI_3$ could also explain origin of a high static dielectric constant [6], degradation of electrical properties [19] or a giant switchable photovoltaic effect [20]. Therefore, the further studies of ions in trihalide perovskite structures are crucial for detailed understanding of all photoelectric processes which determine the efficiency of solar cells.

The family of perovskite materials has been examined for decades. It is well known that oxide–perovskites exhibit ionic conductivity properties associated with mobile oxygen vacancies [21, 22]. The investigation of halide–type perovskites also suggests a high ionic conductivity caused by the migration of halide ions vacancies [23]. The recent studies of the most popular photovoltaic perovskite $MAPbI_3$ (where MA stands for CH_3NH_3) imply that this material is a mixed ionic and electronic conductor [24, 25, 26]. However, the nature of ionic migration needs a better understanding.

In hybrid organic–inorganic perovskites, the transitions from the orthorhombic to tetragonal phase and from the tetragonal to cubic phase were observed [27, 28, 29]. It has been already demonstrated that the change of phase has a great impact not only on the properties of material, like a mobility of charge carriers, a diffusion length or a recombinations rate [30] but also on the conductivity [31]. However, as to our knowledge, there are no reports with measurements of separated electronic and ionic partial conductivities which can indicate the phase transitions.

The aim of this paper is to investigate the electronic and the ionic conductivities in $MAPbI_{3-x}Cl_x$ halide perovskite. In order to separate both conductivities, we have decided to use the modified DC Hebb–Wagner polarization method. In the method, under the steady–state condition, only one type of charge carrier

can flow through electrodes while the other is blocked by either ion or electron blocking material [32, 33, 34, 35, 36]. Recently, this experimental technique was successfully applied to determine the partial conductivities in other materials [22, 37].

2. MATERIALS AND EXPERIMENTAL METHODS

2.1. The perovskite synthesis and film fabrication

The perovskite $MAPbI_{3-x}Cl_x$ precursor was prepared with the following procedure. The commercial Methyloamine (33 wt % in ethanol) from Sigma Aldrich, hydroiodic acid (57 wt % in water) from Alfa Aesar, lead (II) chloride ($PbCl_2$) (99 %) from Acros Organics, ethanol, dimethylformamide (DMF) and diethyl ether have been used. To obtain methylammonium iodide (MAI) powder, methyloamine and hydroiodic acid were mixed in round–bottom flask in 1:1 molar ratio with 100 mL of ethanol. The stirring has been continued for 2 hours in the ice bath due to the exothermic nature of reaction, and evaporated at 50°C afterwards. The precipitate was washed with diethyl ether three times and dried overnight. The readily synthesized MAI and $PbCl_2$ were mixed in 3:1 molar ratio in DMF. After optimization procedures, the most stable films in measurements conditions have been fabricated from 60 wt % precursor concentration. The prepared precursor was used for perovskite preparation in all the experimental section.

The 15 x 20 mm glasses have been cleaned by sonication (10 minutes) with solution of Hellmanex 1 % and later rinsed with hot distilled water. Next, the substrates were placed in ultrasonic bath with isopropyl alcohol and later dried in air. The volume of 60 μL perovskite 60 wt % precursor has been spin–coated with 2100 rpm for 30 s onto the precleaned glasses. The film was annealed for 60 min in air at 100°C. At the substrate with perovskite layer, Al electrode has been thermally evaporated under vacuum 2×10^{-2} Torr with thickness of 50 nm. The mask was used to define two 3 mm electrodes with 3 mm width and 0.5 mm space in between which was an active area of the sample. Finally, the film has been covered with glass cover slips with epoxy resin to prevent the degradation process by contact with air and water during the process of measurements. The resin was placed in a way it did not contact an active area of the sample.

2.2. X–ray diffraction

X–ray diffraction (XRD) measurements have been performed for samples spin–coated on the glass substrate in air using the X–Pert Pro MPD Philips diffractometer at room temperature with $Cu_{K\alpha}$ (1.542 Å). The accelerating voltage and electrical current were 40 kV and 30 mA, respectively. XRD data have been recorded from 10° to 60° for 2θ with the step size of 0.027°.

2.3. SEM images

To analyze the surface morphology and average crystallite size of perovskite films, the FEI Quanta FEG 250 Scanning Electron Microscope (SEM) was used, operating with secondary electron detector in a high vacuum mode with the accelerating voltage of 20 kV.

2.4. Profilometer

The actual thickness of a spin–coated perovskite layer on the substrate with the aluminum electrodes has been measured with the use of surface Tencor Alpha Step 500 Profiler.

2.5. Electrical measurements

The temperature dependence of conductivity has been studied by DC two–wire (2W) method in a temperature range of 77–420 K. In order to perform the DC Hebb–Wagner polarization technique, the thick and dense layer of ion–blocking electrode (a carbon paste from Leit C Conducting Carbon Cement) has been covered on the aluminum electrodes. For the non ion–blocking electrode, a porous silver paste was used as a current collector which was previously reported by Maeda *et al.* [38]. The platinum wires were used as electrical connections. To control the temperature, K–type thermocouple (Keysight 34970A) has been placed right beside the sample in the holder. In the first part of experiment, the measurement cell was located in the tube immersed in a liquid nitrogen. Then the temperature slowly increased. At a high temperature regime (above a room temperature), the tube was heated on the hot–plate as it reached aimed temperature. We did not illuminate our samples during experiment (dark conditions). Performing the electrical measurements (Keithley 2401), the current–voltage characteristics have been taken under steady–state conditions. The conductivities were calculated from the I–V linear relations at low–voltage region.

3. RESULTS AND DISCUSSION

In order to analyze the crystal structure and phase composition of the samples, the XRD measurements were conducted. Figure 1(a) shows X–ray diffraction pattern for the $MAPbI_{3-x}Cl_x$ film on glass substrate which exhibits tetragonal structure with a $I4cm$ symmetry [27]. The following diffraction peaks corresponding to (110), (200), (211), (220), (310), (312), (224), (330) and (440) planes of perovskite material were observed [39, 40]. The highest intensity of 13.93° peak suggests that the orientation of the polycrystalline perovskite film is (110) [41]. In the diffraction pattern, there is no secondary phase from PbI_2 at 12.3° which suggests high purity of the sample [42]. The degradation effect with the XRD has been measured for one sample, results are shown in Figure S1 (Supplementary material). After three weeks from preparing of the sample, there are no visible impurities from PbI_2.

The active area of samples is defined in between two parallel electrodes. From the observation of the surface morphology, we can clearly see a percolation path for charge carriers between crystallites, Figure 1(b). Therefore, the method of spin–coating for a film formation is good enough for the purpose of the paper. The grain size of the polycrystalline material (3.3 ± 0.6) μm has been estimated from the analysis of SEM image. The thickness of the sample obtained from profilometer is (1.80 ± 0.07) μm. The ratio of grain sizes to grain boundaries is very high, therefore in the further part of the paper, we may ignore influence of partial grain boundary conductivity on total conductivity.

In order to check the electrical properties of the $MAPbI_{3-x}Cl_x$ material, the temperature dependence of total and partial surface conductivities have been measured. The total conductivity (σ_{tot}) of material is defined as a sum of electronic and ionic conductivities

$$\sigma_{tot} = \sigma_{el} + \sigma_{ion}, \tag{1}$$

where electronic conductivity (σ_{el}) is associated with electrons and holes, and ionic conductivity (σ_{ion}) relates, in general, to anions and cations.

It should be mentioned that $MAPbI_{3-x}Cl_x$ perovskite is a mateial with addition of chloride salts to precursor for film fabrication. It is known, that the addition of chloride ions improves the stability against humidity [43]. However, only small amount of Cl atoms are present in mixed–halide film [44] and, the chloride doping has a small impact on transport properties [45]. Therefore, only iodide ions are considered in partial conductivity of the studied material.

Figure 2(a) shows the result of the total conductivity in 80–420 K temperature range. Ten samples were measured in the same conditions with 2W method. The conductivity has been calculated from linear fitting of I–V characteristics. In Figure S2 (Supplementary material), there are presented two example measurements for different applied voltage ranges which show linear relation with current. The two–points method is used instead of the four–point (4W) due to the large resistance of the sample in contrast to wires. All of the measurements exhibit the same tendency, thus only one representative result is presented in the paper. At low temperature, we notice a value of conductivity characteristic for insulator materials: 1.77×10^{-6} S m^{-1}. The drastic rise of the total electrical conductivity level is observed at 230 K and at 300 K. It reaches 2.4×10^{-2} S m^{-1} which is of the same order of magnitude as previously reported for trihalide perovskite by Maeda *et al.* [38]. It should be also mentioned that the significant increase of total conductivity, by about four orders of magnitude, has been recently observed by Khenkin et al. [46] and Peng et al. [47] for the transition from orthorhombic to tetragonal phase. Slightly over the room temperature, the conductivity decreases up to 340 K and continues to increase afterwards. Such a significant change in electrical conductivity as a function of temperature may be explained by the phase transition which occurs in the sample.

In order to calculate an activation energy (E_a) for conductivity with tem-

perature, we use the Arrhenius equation

$$\sigma = \sigma_0 \exp\left(-\frac{E_a}{k_B T}\right), \tag{2}$$

where σ is a conductivity of the sample, σ_0 is a pre–exponential factor, whereas k_B and T are the Boltzmann constant and the temperature of the sample, respectively. Figure 2(b) illustrates the total conductivity vs 1000 T^{-1} for the analyzed sample. As can be seen, the linear fitting is in a good agreement with Eq. (2), what proves the validity of thermally active conductivity model. Moreover, the three characteristic regimes can be visible in Figure 2(b). These regimes are related to the phase transitions and, in a consequence, to different crystal forms of the same sample. For the seek of the following paper, the orthorhombic, tetragonal and cubic phases are also called α, β and γ, respectively.

At low temperatures, we notice a negligible change of the total electrical conductivity as temperature increases (Figure 2(b)). Therefore, a very small (even close to zero) activation energy for mixed conductivity has been obtained at α phase. The drastic increase of conductivity occurs at the transition from α to β phase which leads to higher activation energy (0.87 ± 0.02) eV. The transition for trihalide perovskite is expected at 160 K. However, Li *et al.* [48] have presented that the increasing of sample thickness (a distance between electrodes for the volume electrical conduction) from 30 nm to 400 nm can drastically change the temperature of the transition for about 40 K. The distance between both electrodes for our samples (a case of the surface conduction) is around 0.5 mm, what should lead to higher temperature of the phase transition (in our case ∼ 230 K). It is known that the electronic conductivity depends on the mobility of charge carriers. However, Milot *et al.* [30] have reported that the mobility decreases for the transition from orthorhombic to tetragonal phase. Therefore, the change of conductivity should be related to the change of charge carriers concentration. The α and β phases are characterized by the symmetries $Pnma$ and $I4cm$, respectively. A change of the symmetry in phase transition could explain the increase of electrons and holes concentration [49]. For higher temperature, we have recorded a phase transition from β to γ associated with the decrease of activation energy (0.63 ± 0.01) eV. Additionally, the total conductivity drops by about two orders of magnitude (Figure 2(b)). It also seems that the change of perovskite phase is spread over a wide range of temperature. Therefore, it may suggest presence of two phases in temperature between 300 K to about 340 K [50, 51, 52].

It is possible to separate the ionic and the electronic conductivities using the modified DC Hebb–Wagner polarization method under the steady–state condition. Figure S3 (Supplementary material) shows I–V characteristics which have been taken before immersing the sample to liquid nitrogen and just after the room temperature has been reached. The stability analysis were also done in low temperature for a few hours (results not shown here). The lack of differences support the conclusion that the steady-state is obtained for every point of measurements. The temperature dependences of σ_{tot}, σ_{el} and σ_{ion} for tetragonal phase are shown in Figure 3. The representative results for the total

and electronic conductivities are presented without and with the ion–blocking electrode, respectively. For β phase the ionic conductivity takes over the dominance in $MAPbI_{3-x}Cl_x$ perovskite, Figure 3(a). Then, the partial conductivity of iodide ions is one order of magnitude higher than electronic conductivity at room temperature. Let us consider an unintentional doping level (E_c-E_f) which according to Kim et al. [53] is shallow as 0.34 eV below the edge of conduction band (E_c) for $MAPbI_3$. The electron concentration generated by unintentional doping can be defined as

$$n_0 = N_c \exp\left(-\frac{E_c - E_f}{k_B T}\right), \tag{3}$$

where N_c is an effective density of states in conduction band (8.1×10^{24} m^{-3} [54]). Eq. (3) gives $n_0 = 1.57\times10^{19}$ m^{-3}. Taking into account the electron mobility equal to 35 cm^2 V s^{-1} [30], we obtain a value of the electron conductivity equal to 8.83×10^{-3} S m^{-1} which is close to the experimental data at 300 K, see Fig. 3. In reference to these results, it can be stated that $MAPbI_{3-x}Cl_x$ is a mixed ionic–electronic conductor with predominant iodide ions conductivity at tetragonal phase. We suggest that the domination of ions at room temperature may explain the observed effect of hysteresis in trihalide perovskites.

The activation energies for both partial conductivities have been calculated from Eq. (2). The linear correlation coefficient for Arrhenius plot is 0.97. Figure 3(b) shows that, for tetragonal phase, the activation energy drastically increases for both ionic and electronic charge carriers to the values of (0.87 ± 0.02) eV and (1.12 ± 0.03) eV, respectively. The obtained result of the activation energy for migration of iodide ions is similar to previous reports for the halide inorganic perovskites with anion vacancy transportation mechanism [23, 55, 56] and for the methylammonium lead iodide perovskite [26]. We can see that the ionic conductivity dominates for β phase. However, its activation energy is lower in respect to the electronic conductivity. Eames *et al.* [26] have assumed that the only possible mechanism for transport of ions in $MAPbI_{3-x}Cl_x$ perovskite is by hopping between the neighbouring vacancies which needs low activation energy. Motta *et al.* [45] have proposed that the bottom of conduction band and the top of valence band for $CH_3NH_3PbI_{3-x}Cl_x$ originate from p orbitals of Pb atom and p orbitals of I atom, respectively. Therefore, the creation of electrons and holes and, as a consequence, also their transport (the bandpass transportation mechanism) require a higher thermal energy. That may explain the higher value of activation energy observed for the electronic conduction in comparison to the ionic conduction mechanism.

4. CONCLUSIONS

In summary, we have studied a temperature dependence of the total conductivity for the trihalide perovskite $CH_3NH_3PbI_{3-x}Cl_x$. The obtained results clearly demonstrate the orthorhombic to tetragonal phase and the tetragonal to cubic phase transitions. Our analysis suggests the domination of ionic charge

carriers in the tetragonal phase. We have proposed the explanation based on the hopping mechanism of ions and bandpass mechanism for electronic charge carriers. It is implied that the high partial ionic conductivity at a room temperature might be a possible explanation of the parasitic effect of hysteresis in trihalide perovskite solar cells which is potentially a problem in a wider application of these perovskite materials. Also, it should be pointed out that there are still much unresolved issues with the perovskite material and the next step should concern analysis of ion conductivity for orthorhombic and cubic phase to get better understanding of the material physics.

5. Supplementary material

Supplementary material (XRD degradation results and I–V curves in temperatures) associated with this article can be found, in the online version, at ...

[1] M. Saliba, T. Matsui, K. Domanski, J.-Y. Seo, A. Ummadisingu, S. M. Zakeeruddin, J.-P. Correa-Baena, W. R. Tress, A. Abate, A. Hagfeldt, M. Grätzel, Incorporation of Rubidium Cations into Perovskite Solar Cells Improves Photovoltaic Performance, Science 354 (6309).

[2] X. Zhu, D. Yang, R. Yang, B. Yang, Z. Yang, X. Ren, J. Zhang, J. Niu, J. Feng, S. F. Liu, Superior Stability for Perovskite Solar Cells with 20% Efficiency Using Vacuum Co-evaporation, Nanoscale 9 (34) (2017) 12316–12323.

[3] Y. M. Wang, S. Bai, L. Cheng, N. N. Wang, J. P. Wang, F. Gao, W. Huang, High-Efficiency Flexible Solar Cells Based on Organometal Halide Perovskites, Adv. Mater. 28 (22) (2016) 4532–4540.

[4] T. Leijtens, S. D. Stranks, G. E. Eperon, R. Lindblad, E. M. J. Johansson, I. J. McPherson, H. Rensmo, J. M. Ball, M. M. Lee, H. J. Snaith, Electronic Properties of Meso-Superstructured and Planar Organometal Halide Perovskite Films: Charge Trapping, Photodoping, and Carrier Mobility, ACS Nano 8 (7) (2014) 7147–7155.

[5] A. Miyata, A. Mitioglu, P. Plochocka, O. Portugall, J. T.-W. Wang, S. D. Stranks, H. J. Snaith, R. J. Nicholas, Direct Measurement of the Exciton Binding Energy and Effective Masses for Charge Carriers in Organic-Inorganic Tri-halide Perovskites, Nat. Phys. 11 (7) (2015) 582–587.

[6] Q. Lin, A. Armin, R. C. R. Nagiri, P. L. Burn, P. Meredith, Electro-Optics of Perovskite Solar Cells, Nat. Photonics 9 (2) (2015) 106–112.

[7] S. D. Stranks, G. E. Eperon, G. Grancini, C. Menelaou, M. J. P. Alcocer, T. Leijtens, L. M. Herz, A. Petrozza, H. J. Snaith, Electron-Hole Diffusion Lengths Exceeding 1 Micrometer in an Organometal Trihalide Perovskite Absorber, Science 342 (6156) (2013) 341–344.

[8] X. Ren, Z. Wang, W. E. Sha, W. C. Choy, Exploring the Way To Approach the Efficiency Limit of Perovskite Solar Cells by Drift-Diffusion Model, ACS Photonics 4 (4) (2017) 934–942.

[9] W. E. I. Sha, X. Ren, L. Chen, W. C. H. Choy, The Efficiency Limit of $CH_3NH_3PbI_3$ Perovskite Solar Cells, Appl. Phys. Lett. 106 (22) (2015) 221104.

[10] H. J. Snaith, A. Abate, J. M. Ball, G. E. Eperon, T. Leijtens, N. K. Noel, S. D. Stranks, J. T. W. Wang, K. Wojciechowski, W. Zhang, Anomalous Hysteresis in Perovskite Solar Cells, J. Phys. Chem. Lett. 5 (9) (2014) 1511–1515.

[11] A. K. Jena, H.-W. Chen, A. Kogo, Y. Sanehira, M. Ikegami, T. Miyasaka, The Interface between FTO and the TiO_2 Compact Layer Can Be One of the Origins to Hysteresis in Planar Heterojunction Perovskite Solar Cells, ACS Appl. Mater. Interfaces 7 (18) (2015) 9817–9823.

[12] B. Chen, M. Yang, S. Priya, K. Zhu, Origin of J-V Hysteresis in Perovskite Solar Cells, J. Phys. Chem. Lett. 7 (5) (2016) 905–917.

[13] L. Cojocaru, S. Uchida, P. V. V. Jayaweera, S. Kaneko, J. Nakazaki, T. Kubo, H. Segawa, Origin of the Hysteresis in I V Curves for Planar Structure Perovskite Solar Cells Rationalized with a Surface Boundary-induced Capacitance Model, Chem. Lett. 44 (12) (2015) 1750–1752.

[14] S. van Reenen, M. Kemerink, H. J. Snaith, Modeling Anomalous Hysteresis in Perovskite Solar Cells, J. Phys. Chem. Lett. 6 (19) (2015) 3808–3814.

[15] W. Tress, N. Marinova, T. Moehl, S. M. Zakeeruddin, M. K. Nazeeruddin, M. Gratzel, Understanding the Rate-Dependent J-V Hysteresis, Slow Time Component, and Aging in $CH_3NH_3PbI_3$ Perovskite Solar Cells: the Role of a Compensated Electric Field, Energy Environ. Sci. 8 (3) (2015) 995–1004.

[16] S. G, P. Mahale, B. P. Kore, S. Mukherjee, M. S. Pavan, C. De, S. Ghara, A. Sundaresan, A. Pandey, T. N. Guru Row, D. D. Sarma, Is $CH_3NH_3PbI_3$ Polar?, J. Phys. Chem. Lett. 7 (13) (2016) 2412–2419.

[17] H. Röhm, T. Leonhard, M. J. Hoffmann, A. Colsmann, Ferroelectric domains in methylammonium lead iodide perovskite thin-films, Energy Environ. Sci. 10 (4) (2017) 950–955.

[18] A. M. A. Leguy, J. M. Frost, A. P. McMahon, V. G. Sakai, W. Kochelmann, C. Law, X. Li, F. Foglia, A. Walsh, B. C. O'Regan, J. Nelson, J. T. Cabral, P. R. F. Barnes, The Dynamics of Methylammonium Ions in Hybrid Organic-Inorganic Perovskite Solar Cells, Nat. Commun. 6 (2015) 7124.

[19] S. Kim, S. Bae, S. W. Lee, K. Cho, K. D. Lee, H. Kim, S. Park, G. Kwon, S. W. Ahn, H. M. Lee, Y. Kang, H. S. Lee, D. Kim, Relationship between ion migration and interfacial degradation of CH3NH3PbI3perovskite solar cells under thermal conditions, Sci. Rep. 7 (1) (2017) 1–9.

[20] Z. Xiao, Y. Yuan, Y. Shao, Q. Wang, Q. Dong, C. Bi, P. Sharma, A. Gruverman, J. Huang, Giant switchable photovoltaic effect in organometal trihalide perovskite devices, Nat. Mater. 14 (2) (2015) 193–197.

[21] J. B. Goodenough, Electronic and Ionic Transport Properties and Other Physical Aspects of Perovskites, Rep. Prog. Phys. 67 (11) (2004) 1915–1993.

[22] T. Miruszewski, J. Karczewski, B. Bochentyn, P. Jasinski, M. Gazda, B. Kusz, Determination of the Ionic Conductivity of Sr-doped Lanthanum Manganite by Modified Hebb-Wagner Technique, J. Phys. Chem. Solids 91 (2016) 163–169.

[23] J. Mizusaki, K. Arai, K. Fueki, Ionic Conduction of the Perovskite-Type Halides, Solid State Ion. 11 (3) (1983) 203–211.

[24] A. Dualeh, T. Moehl, N. Tétreault, J. Teuscher, P. Gao, M. K. Nazeeruddin, M. Grätzel, Impedance Spectroscopic Analysis of Lead Iodide Perovskite-Sensitized Solid-State Solar Cells, ACS Nano 8 (1) (2014) 362–373.

[25] P. Calado, A. M. Telford, D. Bryant, X. Li, J. Nelson, B. C. O'Regan, P. R. Barnes, Evidence for Ion Migration in Hybrid Perovskite Solar Cells with Minimal Hysteresis, Nat. Commun. 7 (2016) 13831.

[26] C. Eames, J. M. Frost, P. R. F. Barnes, B. C. O'Regan, A. Walsh, M. S. Islam, Ionic Ttransport in Hybrid Lead Iodide Perovskite Solar Cells, Nat. Commun. 6 (2015) 7497.

[27] T. Baikie, Y. Fang, J. M. Kadro, M. Schreyer, F. Wei, S. G. Mhaisalkar, M. Graetzel, T. J. White, Synthesis and Crystal Chemistry of the Hybrid Perovskite $(CH_3NH_3)PbI_3$) for Solid-State Sensitised Solar Cell Applications, J. Mater. Chem. A 1 (18) (2013) 5628.

[28] Y. Kawamura, H. Mashiyama, K. Hasebe, Structural Study on Cubic-Tetragonal Transition of $CH_3NH_3PbI_3$, J. Phys. Soc. Jpn. 71 (7) (2002) 1694–1697.

[29] A. Maalej, Y. Abid, A. Kallel, A. Daoud, A. Lautié, F. Romain, Phase Transitions and Crystal Dynamics in the Cubic Perovskite $CH_3NH_3PbCl_3$, Solid State Commun. 103 (5) (1997) 279–284.

[30] R. L. Milot, G. E. Eperon, H. J. Snaith, M. B. Johnston, L. M. Herz, Temperature-Dependent Charge-Carrier Dynamics in $CH_3NH_3PbI_3$ Perovskite Thin Films, Adv. Funct. Mater. 25 (39) (2015) 6218–6227.

[31] A. Slonopas, B. J. Foley, J. J. Choi, M. C. Gupta, Charge Transport in Bulk $CH_3NH_3PbI_3$ Perovskite, J. Appl. Phys. 119 (7) (2016) 74101.

[32] W. Weppner, R. A. Huggins, Ionic Conductivity of Alkali Metal Chloroaluminates, Phys. Lett. A 58 (4) (1976) 245–248.

[33] I. Riess, Four Point Hebb-Wagner Polarization Method for Determining the Electronic Conductivity in Mixed Ionic-Electronic Conductors, Solid State Ion. 51 (3) (1992) 219–229.

[34] I. Riess, Measurement of Ionic Conductivity in Semiconductors and Metals, Solid State Ion. 44 (3-4) (1991) 199–205.

[35] I. Riess, Review of the Limitation of the Hebb-Wagner Polarization Method for Measuring Partial Conductivities in Mixed Ionic Electronic Conductors, Solid State Ion. 91 (3-4) (1996) 221–232.

[36] K. C. Lee, H. I. Yoo, Hebb-Wagner-Type Polarization/Relaxation in the Presence of the Cross Effect Between Electronic and Ionic Flows in a Mixed Conductor, J. Phys. Chem. Solids 60 (7) (1999) 911–927.

[37] K. H. Kim, T. Lee, W. Joo, H. I. Yoo, Current vs. Voltage Behavior of Hebb-Wagner Ion-Blocking Cell through Compound ($Bi_{1.46}Y_{0.54}O_3$) Decomposition and Decomposition Kinetics, Solid State Ion. 267 (2014) 9–15.

[38] M. Maeda, M. Hattori, A. Hotta, I. Suzuki, Dielectric Studies on $CH_3NH_3PbX_3$ (X = Cl and Br) Single Cystals, J. Phys. Soc. Jpn. 66 (5) (1997) 1508–1511.

[39] Z.-L. Tseng, C.-H. Chiang, C.-G. Wu, Surface Engineering of ZnO Thin Film for High Efficiency Planar Perovskite Solar Cells, Sci. Rep. 5 (2015) 13211.

[40] H.-B. Kim, H. Choi, J. Jeong, S. Kim, B. Walker, S. Song, J. Y. Kim, Mixed Solvents for the Optimization of Morphology in Solution-Processed, Inverted-Type Perovskite/Fullerene Hybrid Solar Cells, Nanoscale 6 (12) (2014) 6679–6683.

[41] J. Lian, Q. Wang, Y. Yuan, Y. Shao, J. Huang, Organic Solvent Vapor Sensitive Methylammonium Lead Trihalide Film Formation for Efficient Hybrid Perovskite Solar Cells, J. Mater. Chem. A 3 (17) (2015) 9146–9151.

[42] K. Wu, A. Bera, C. Ma, Y. Du, Y. Yang, L. Li, T. Wu, Temperature-Dependent Excitonic Photoluminescence of Hybrid Organometal Halide Perovskite Films, Phys. Chem. Chem. Phys. 16 (41) (2014) 22476–22481.

[43] D. Koushik, W. J. H. Verhees, Y. Kuang, S. Veenstra, D. Zhang, M. A. Verheijen, M. Creatore, R. E. I. Schropp, High-Efficiency Humidity-Stable Planar Perovskite Solar Cells Based on Atomic Layer Architecture, Energy Environ. Sci. 10 (1) (2017) 91–100.

[44] H. Yu, F. Wang, F. Xie, W. Li, J. Chen, N. Zhao, The Role of Chlorine in the Formation Process of "$CH_3NH_3PbI_{3-x}Cl_x$" Perovskite, Adv. Funct. Mater. 24 (45) (2014) 7102–7108.

[45] C. Motta, F. El-Mellouhi, S. Sanvito, Charge Carrier Mobility in Hybrid Halide Perovskites, Sci. Rep. 5 (1) (2015) 12746.

[46] M. V. Khenkin, D. V. Amasev, S. A. Kozyukhin, A. V. Sadovnikov, E. A. Katz, A. G. Kazanskii, Temperature and spectral dependence of $CH_3NH_3)PbI_3$ films photoconductivity, Applied Physics Letters 110 (22) (2017) 222107.

[47] W. Peng, J. Yin, K. T. Ho, O. Ouellette, M. De Bastiani, B. Murali, O. El Tall, C. Shen, X. Miao, J. Pan, E. Alarousu, J. H. He, B. S. Ooi, O. F. Mohammed, E. Sargent, O. M. Bakr, Ultralow Self-Doping in Two-dimensional Hybrid Perovskite Single Crystals, Nano Lett. 17 (8) (2017) 4759–4767.

[48] D. Li, W. Gongming, C. Hung-Chieh, C. Chih-Yen, W. Hao, L. Yuan, H. Yu, D. Xiangfeng, Size-dependent phase transition in methylammonium lead iodide perovskite microplate crystals, Nat. Commun. 9 (2016) 11330.

[49] P. S. Whitfield, N. Herron, W. E. Guise, K. Page, Y. Q. Cheng, I. Milas, M. K. Crawford, Structures, Phase Transitions and Tricritical Behavior of the Hybrid Perovskite Methyl Ammonium Lead Iodide, Sci. Rep. 6 (2016) 35685.

[50] A. Dobrovolsky, A. Merdasa, E. L. Unger, A. Yartsev, I. G. Scheblykin, Defect-induced local variation of crystal phase transition temperature in metal-halide perovskites, Nature Communications 8 (1) (2017) 1–7.

[51] N. Onoda-Yamamuro, T. Matsuo, H. Suga, Dielectric Study of CH3NH3PbX3 (X = Cl, Br, I), J. Phys. Chem. Solids 53 (7) (1992) 935–939.

[52] V. D'Innocenzo, G. Grancini, M. J. P. Alcocer, A. R. S. Kandada, S. D. Stranks, M. M. Lee, G. Lanzani, H. J. Snaith, A. Petrozza, Excitons versus free charges in organo-lead tri-halide perovskites, Nat. Commun. 5 (2014) 3586.

[53] H. D. Kim, H. Ohkita, H. Benten, S. Ito, Photovoltaic Performance of Perovskite Solar Cells with Different Grain Sizes, Adv. Mater. 28 (5) (2016) 917–922.

[54] T. S. Sherkar, C. Momblona, L. Gil-Escrig, H. J. Bolink, L. J. A. Koster, Improving Perovskite Solar Cells: Insights From a Validated Device Model, Adv. Energy Mater. 7 (13).

[55] R. L. Narayan, S. V. Suryanarayana, Transport Properties of the Perovskite-Type Halides, Mater. Lett. 11 (8-9) (1991) 305–308.

[56] T. Kuku, Ionic Transport and Galvanic Cell Discharge Characteristics of $CuPbI_3$ Thin Films, Thin Solid Films 325 (1-2) (1998) 246–250.

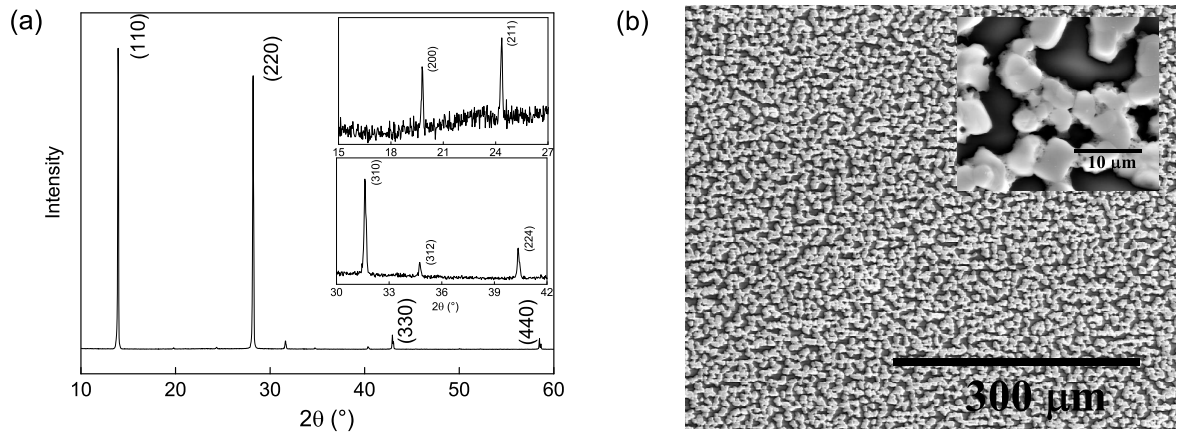

Figure 1: Structural results for $MAPbI_{3-x}Cl_x$ sample. (a) X–ray diffraction pattern, and (b) Scanning Electron Microscopy (SEM) image.

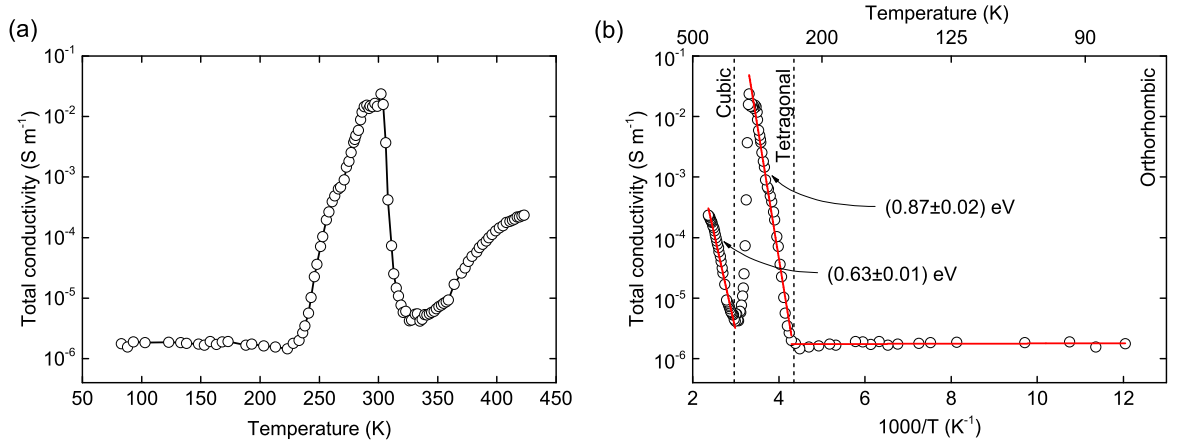

Figure 2: The temperature dependence of total electrical conductivity for $MAPbI_{3-x}Cl_x$ sample. (a) Conductivity as a function of temperature in absolute scale, and (b) Arrhenius plot of total conductivity with activation energy given for each crystallographic phases.

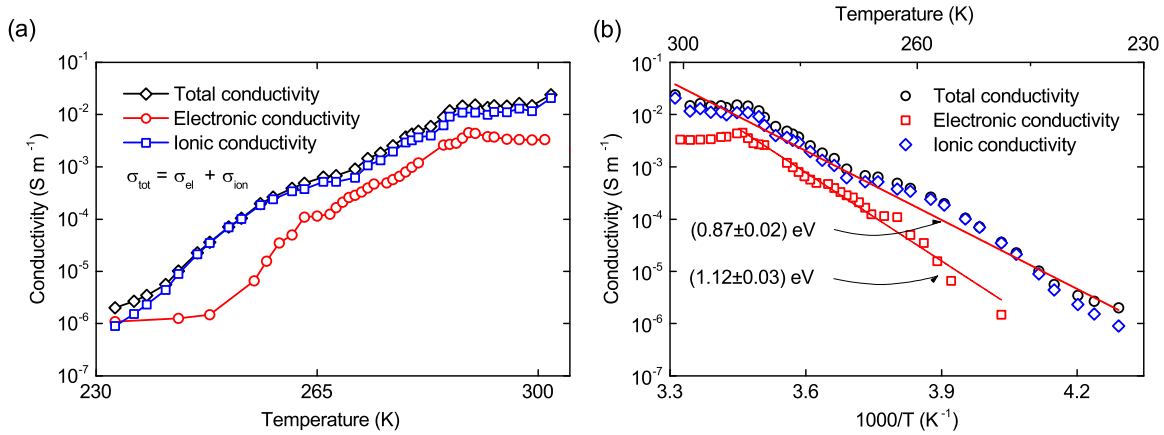

Figure 3: The total conductivity and partial electronic and ionic conductivities presented for β phase of $MAPbI_{3-x}Cl_x$ sample. (a) Conductivities as a function of temperature in absolute scale, (b) Arrhenius plot for partial ionic and electronic conductivities.